BULLETIN OF THE POLISH ACADEMY OF SCIENCES
TECHNICAL SCIENCES, Vol. 63, No. 1, 2015
DOI: 10.1515/bpasts-2015-0020

Optimization of two-component armour

P. KĘDZIERSKI*, A. MORKA, G. SŁAWIŃSKI, and T. NIEZGODA

Department of Mechanics and Applied Computer Science, Faculty of Mechanical Engineering, Military University of Technology, 2 Kaliskiego St., 00-908 Warsaw, Poland

Abstract. The paper presents research on optimization of two-layer armour subjected to the normal impact of the 7.62x54 B32 armour piercing (AP) projectile. There were analysed two cases in which alumina Al_2O_3 was supported by aluminium alloy AA2024-T3 or armour steel Armox 500T. The thicknesses of layers were determined to minimize the panel areal density whilst satisfying the constraint, which was the maximum projectile velocity after panel perforation. The problem was solved through the utilization of LS-DYNA, LS-OPT and HyperMorph engineering software. The axisymmetric model was applied to the calculation in order to provide sufficient discretization. The response of the aluminium alloy, armour steel and projectile material was described with the Johnson-Cook model, while the one of the alumina with the Johnson-Holmquist model. The study resulted in the development of a panel optimization methodology, which allows the layer thicknesses of the panel with minimum areal density to be determined. The optimization process demonstrated that the areal density of the lightest panel is 71.07 and 71.82 kg/m^2 for Al_2O_3-Armox 500T and Al_2O_3-AA2024-T3, respectively. The results of optimization process were confirmed during the experimental investigation.

Key words: optimization, composites, numerical simulations, ballistic protection.

1. Introduction

One of the main criteria used for comparing armours providing the same level of protection is areal density. A lower panel mass allows a reduction in fuel consumption and preserves the mobility of the vehicle on which it is mounted. One of the methods used to decrease the areal density of the armour is the employment of a two-layer system, in which a hard layer is supported by a plastic one. One layer is designed to erode the projectile, while the other, softer layer, absorbs the kinetic energy of the projectile by plastic deformation [1]. The first ceramic-metal armour was proposed by Wilkins et al. [2]. Many descriptions in the literature indicate the improved efficiency of two-component systems over monolithic metal armours [3–5]. Among the most popular dual hardness panels, there are solutions consisting of alumina supported by the aluminium alloy or steel.

A number of studies can be found in the literature regarding the optimization of two-component armour systems, which generally refer to ceramic/metal armours. The optimization problem has been solved in the literature by both modelling and experimental approaches. The modelling approaches predominantly include analytical methods, which are typically simplified from complex realistic cases. The analytical optimization of ceramic/metal armours is mainly based on the Florence model [6]. The problem of determining the structure of a two-component armour with specific areal density that provides the maximum ballistic limit velocity was considered by Hetherington [7]. Wang and Lu [8] studied a similar problem, in which the total thickness of the armour rather than the areal density was given. Shi and Grow [9] investigated the problem of a two-component armour in which both the total thickness and the areal density were limited. Ben-Dor et al. [10] studied the problem of maximization of the ballistic limit velocity for given areal density or total thickness and minimization of the areal density or the total thickness for the given impact velocity, using an updated version of the Florence model.

The authors have been investigating the optimal thicknesses of armour layers using a coupling of numerical methods, such as the finite element method (FEM) with optimization tools. The paper presents an approach that approximates the objective function with a neural network and then searches for its optimum by applying a hybrid adaptive simulated annealing algorithm (ASA). The study concerned the minimization of the areal density of a two-component armour protecting against a 7.62x54 B32 AP projectile.

2. Problem description

The optimization of a two-layer armour subjected to the normal impact of a 7.62x54 B32 AP projectile was carried out. Calculations were performed for two cases, which differed with the material of the second layer. The target diameter was 50 mm, and the initial velocity of the projectile was equal to 854 m/s. The geometry of the projectile and armour are shown in Fig. 1. The aim of the study was to determine the layer thicknesses providing protection against the assumed projectile. The initial configuration and ranges of layer thicknesses are listed in Table 1.

*e-mail: kedzierski.piotr@wat.edu.pl

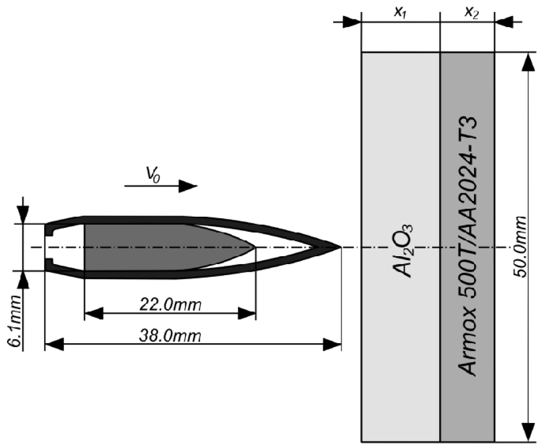

Fig. 1. Configuration of studied problem

Table 1
Ranges of design variables and their initial values

Variant		Range of thickness [mm]		Initial thickness [mm]
1	Al_2O_3 Armox 500T	Al_2O_3	6–10	8
		Armox 500T	3–7	5
2	Al_2O_3 AA2024-T3	Al_2O_3	6–14	10
		AA2024-T3	3–11	7

3. Optimization fundamentals

The issue of optimization can be simplified to determination of the best admissible solutions of a given problem taking into consideration the assumed criterion of quality [11]. The optimization problem is composed of the following elements: the set of design variables (design parameters), the objective function and the constraints. Its solution consists in the identification of a set of design variables that ensure the minimization of the objective function:

$$\min f(\mathbf{x}). \tag{1}$$

Satisfying the constraints:

$$h_k(\mathbf{x}) = 0, \qquad k = 1, 2, ..., l, \tag{2}$$

$$g_j(\mathbf{x}) \leq 0, \qquad j = 1, 2, ..., m. \tag{3}$$

where f, g and h are functions of independent variables x_1, x_2, x_3, $\ldots$, x_n. The function f, referred to as the cost or objective function, identifies the quantity to be minimised or maximised. Functions g and h are constraint functions representing the design restrictions. The variables collectively described by the vector **x** are often referred to as design variables or design parameters. In the considered case the design parameters were the thicknesses of both layers. As it was previously mentioned, the panel areal density was assumed to be the objective function, whose minimum was sought. A limitation was the projectile velocity after panel perforation, which could not exceed 10% of its initial value. The character of the constraint was based on the assumption that the panel was mounted onto a vehicle hull, which provides the primary protection.

Method of problem solution. The optimization calculations were performed using the coupling of LS-DYNA, LS-OPT and HyperMorph. The optimization toolchain is depicted in Fig. 2.

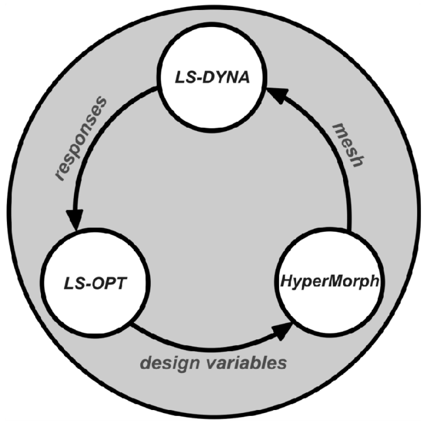

Fig. 2. Optimization toolchain

The LS-OPT package was used to define the optimization problem, monitor the computation and analyse the results. LS-OPT generated sets of design variables (layer thicknesses), for which HyperMorph created meshes of the numerical models. Then, appropriate calculations were conducted in LS-DYNA software with the finite element method. The LS-OPT package searched for the optimal solution employing response surface model RSM, which replaces the actual objective and response functions. In the considered case, the response surface model, which was constructed based on an appropriately selected set of numerical simulations, was a neural network with radial basic functions RBF. The structure of the neural network is shown in Fig. 3 [12]. In calculation, a neural network made of three different layers was utilized. The input layer was linear and a number of its neurons resulted from a number of design variables. A single hidden layer consists of nonlinear neurons described with radial functions. The linear output layer is composed of one neuron, which superimposes signals from the hidden layer giving representation of the object and constraint functions.

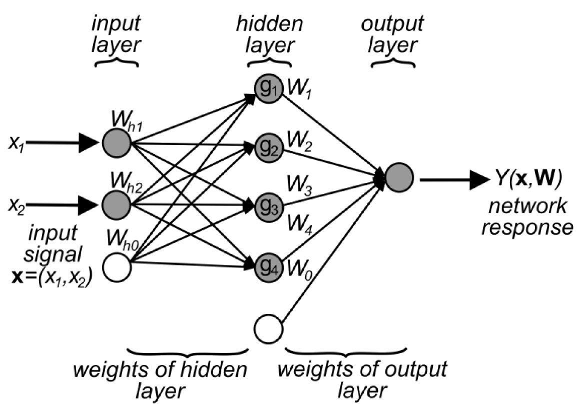

Fig. 3. Radial neural network

An approximation function built on the basis of the neural network, depicted in Fig. 3, has the following form (4):

$$Y(x,W) = W_0 + W_1 g_1 + W_2 g_2 + \cdots + W_H g_H = W_0 + \sum_{h=1}^{H} W_h g_h, \tag{4}$$

where $\mathbf{x} = (x_1, ..., x_n)$ represents vector of design variables, $\mathbf{W}$ is vector of neural network weights, $\mathbf{W}_{hn} = (W_{h1}, ..., W_{hn})$ is vector of hidden layer weights – location of h^{th} RBF centre, W_{h0} controls the smoothness of h^{th} RBF, $\mathbf{W}_h = (W_1, ..., W_h)$ is the vector of output layer weights – weight of h^{th} RBF, W_0 – is bias of approximation function Y and g_h denotes RBF.

Radial functions change radially around the selected centre, each of which corresponds to only a local region of design space [13]. Example of RBF is Hardy's function formulated as follows:

$$g_h(x_1, ..., x_n) = \frac{1}{\sqrt{r^2 + W_{h0}^2}}, \tag{5}$$

where r distance between the input vector of design variables $\mathbf{x}_k = (x_1, \ldots, x_n)$ and the centre of h^{th} RBF $\mathbf{W}_{hn} = (W_{h1}, \ldots, W_{hn})$ in n-dimensional space calculated as:

$$r = \sqrt{\sum_{k=1}^{n} (x_k - W_{hk})^2}. \tag{6}$$

Parameters of the neural network are determined during its training. The learning procedure of RBF network consists of three stages that include: choice of the centres of the hidden radial basis neurons W_{hn}, choice of parameter W_{h0} – smoothness of the radial function for each hidden neuron, determination of the weight factors between hidden and output layer W_h [14]. In the presented case, the panel areal density and results of numerical simulations such as projectile velocity after panel perforation were used for training. An example of the response surface based on a neural network with two radial functions in one-dimensional space is shown in Fig. 4.

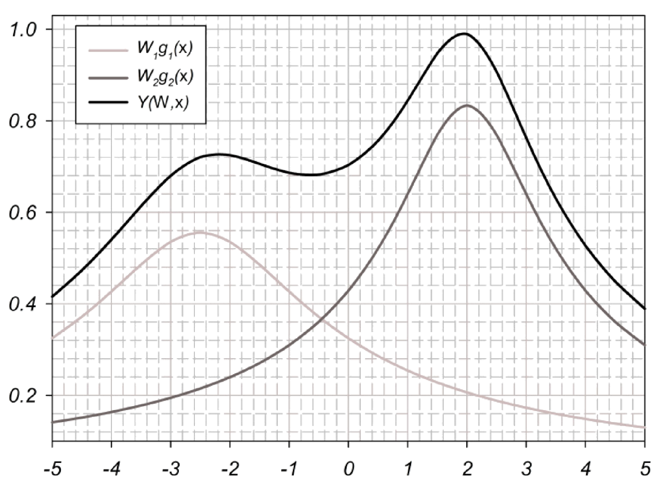

Fig. 4. Approximation with radial neural network

The minimum of the so-defined objective function (4) was found by applying a hybrid ASA algorithm. The hybrid algorithm is a combination of two optimization algorithms: ASA and a leapfrog optimizer for constrained minimization (LFOPC). The adaptive annealing algorithm is a stochastic procedure that makes it possible to find the basin of the objective function in which the global minimum is located [15]. The established solution is the starting point for the gradient-based leapfrog algorithm, which enables the quick and accurate determination of the global optimum [16].

Numerical model description. Numerical calculations were performed with the non-linear finite element code LS-DYNA, which is a commonly used tool for solving problems associated with shock wave propagation, blasts and impacts. An explicit integration scheme was used to solve the equation of motion. An axisymmetric model was built in order to ensure sufficient discretization.

The Johnson-Cook (JC) constitutive model was used to describe the behaviour of the aluminium alloy, armour steel and projectile material. This model is typically applied in the study of explosive metal forming, armour perforation and impacts, i.e., situations that are accompanied by high strain rate deformations. The flow stress in the constitutive relation is expressed as [17]:

$$\sigma_y = (A + B\varepsilon^n)(1 + C \ln \dot{\varepsilon}*)(1 - (T*)^m), \tag{7}$$

where ε is the equivalent plastic strain, $\dot{\varepsilon}$ is the plastic strain-rate, and A, B, C, n, m are material constants. The normalised strain-rate and temperature in Eq. (7) are given in the following forms:

$$\dot{\varepsilon}* = \frac{\dot{\varepsilon}}{\dot{\varepsilon}_0}, \tag{8}$$

$$T* = \frac{(T - T_0)}{(T_m - T_0)}, \tag{9}$$

where $\dot{\varepsilon}_0$ is the quasi-static threshold strain rate, T_0 is the reference temperature, and T_m is the melt temperature.

Pressure occurring during panel perforation is much larger than the yield stress of ductile materials comprising the model, which behave like a compressible liquid. This state is defined as the hydrodynamic regime, and requires a state equation for the determination of the constitutive model. In the constructed model, the Gruneisen equation of state (EOS) was used. The pressure for the compressed material is defined as [18]:

$$p = \frac{\rho_0 C^2 \mu \left[1 + \left(1 - \frac{\gamma_0}{2}\right)\mu \frac{a}{2}\mu^2\right]}{\left[1 - (S_1 - 1)\mu - S_2 \frac{\mu^2}{\mu+1} - S_3 \frac{\mu^3}{(\mu+1)^2}\right]^2} + (\gamma_0 + a\mu)E \tag{10}$$

and for expanded materials:

$$p = \rho_0 C^2 \mu + (\gamma_0 + a\mu)E, \tag{11}$$

where C is the bulk speed of sound, ρ_0 is the initial density, γ_0 is the Gruneisen gamma, a is the first order volume correction to γ_0, S_1, S_2, S_3 are the coefficients of the slope of the shock wave velocity – particle velocity curve, and E is internal energy, $\mu = (\rho/\rho_0) - 1$.The material data for the JC model and the Gruneisen EOS applied in this work are listed in Table 2 [19–23].

Table 2
JC model and Gruneisen EOS parameters for core, jacket, aluminium alloy and armour steel

Name	Symbol	Unit	Core	Jacket	AA2024-T3	Armox 500T
Source	N/A	N/A	[19, 20]	[21]	[22, 23]	[19, 20]
mass density	RO	g/cm^3	7.85	8.8	2.81	7.85
shear modulus	G	GPa	79.6	44	28.6	79.6
Young's modulus	E	GPa	N/A	N/A	N/A	N/A
Poisson's ratio	PR	–	N/A	N/A	N/A	N/A
JC:						
	A	GPa	1.576^a	0.112	0.369	0.849
	B	GPa	2.906^a	0.505	0.684	1.34
	N	–	0.1172^a	0.42	0.73	0.0923
	C	–	0.00541	0.009	0.0083	0.00541
	M	–	0.87	1.68	1.7	0.87
melt temperature	TM	K	1800	1030	775	1800
room temperature	TR	K	293	293	293	293
referential strain rate	EPSO	1/s	1	1	10	1
specific heat	CP	J/kgK	450	376	875	450
Gruneisen EOS:						
	C	m/s	4570	3720	5382	4570
	S1	–	1.49	1.328	1.338	1.49
	S2	–	0	0	0	0
	S3	–	0	0	0	0
	GAMAO	–	1.930	1.657	2	1.93
	A	–	0.5	0	0.48	0.5
JC FAILURE:						
	D1	–	0.0356^a	0.54	-0.07	-0.4^a
	D2	–	0.0826^a	4.89	1.02	1.5^a
	D3	–	-2.5^a	3.03	-1.62	-0.5^a
	D4	–	0	0.014	0	0
	D5	–	0	1.12	0	0

^{a} designated based on conducted experimental tests.

In order to describe the constitutive response of Al_2O_3 ceramics, the Johnson-Holmquist (JH2) model was employed. This model is widely used for modelling the mechanical behaviour of brittle materials, such as ceramics, rock and concrete, for a high range of strain rates. Typically, the Johnson-Holmquist relation is applied while dealing with ballistic impacts on ceramics [24]. The normalised by Hugoniot Elastic Limit (HEL) actual equivalent stress is linearly interpolated from the current values of the normalized intact and fractured strengths [25]:

$$\sigma * = \sigma_i * - D\left(\sigma_i * - \sigma_f *\right), \tag{12}$$

where D is a damage variable, which ranges from 0 for intact material to 1 for fully fractured material. The normalised intact strength is given by:

$$\sigma_i * = A\left(P * + T *\right)^N \left(1 + C \ln \dot{\varepsilon} *\right) \tag{13}$$

and the normalised fracture strength is given by:

$$\sigma_f * = B\left(P *\right)^M \left(1 + C \ln \dot{\varepsilon} *\right), \tag{14}$$

where A, B, C, M and N are material constants, $P*$is the normalised pressure, and $\dot{\varepsilon}*$ is the normalised strain-rate. Most of the material data for the JH model which are given in Table 3, were taken from literature source [26] and the others were designated during calibration of a numerical model reproducing bending and compression experimental tests. Noteworthy is the average value of tensile strength T deviating from properties of the best alumina commercially available.

Table 3
JH2 model parameters for ceramics

Name	Symbol	Unit	Ceramics Al_2O_3
mass density	RO	g/cm^3	3.89
shear modulus	G	GPa	152
JH2:			
	A	-	1.056^a
	B	-	0.45
	C	-	0.007
	M	-	0.6
	N	-	0.64
	EPSI	1/s	1
	T	GPa	0.120^a
	SFMAX	-	1
	HEL	GPa	9^a
	BETA	-	1
EOS:			
	K1	GPa	231
	K2	GPa	-160
	K3	GPa	2774
JH2 FAILURE:			
	D1	-	0.0125
	D2	-	0.7

^{a} designated based on conducted experimental tests.

Boundary conditions introduced in the model provided the panel fixing. A support in the simulation was implemented by removing the degrees of freedom from some of the nodes located on the rear surface of each plate.

An initial condition in the model was that the velocity of the projectile, which was set to be equal to 854 m/s.

Discussion of optimization results. The approximation of the objective and the constraint function is depicted in Figs. 5 and 6, respectively. As a measure of the accuracy of the response surface, the root mean square (RMS) error between the predicted and computed values was adopted:

$$RMS = \sqrt{\frac{1}{P}\sum_{i=1}^{P}\left(\widehat{y}_i - y_i\right)^2}, \tag{15}$$

where P is a number of numerical experiments, y_i the results of the numerical simulations, and $\widehat{y}_i$ the predicted values with the response surface model. The error of objective function RMS, depending on the variant, ranged from 0.000025 to 0.000394 kg/m^2. In contrast, the RMS error for the constraint function ranged from 22.9 to 77.4 m/s. In the case of the objective function, the response surface model based on neural network maps the panel areal density precisely as evidenced by the negligible small RMS error. Panel areal density, as the sum of the products of the layer thicknesses and their volume density, is a linear dependence, which neural networks learn fast and efficiently. The constraint function approximation with the neural network is not as accurate as the objective function. Discrepancies between the predicted and computed values of constraint come from, among other things, its nonlinear character.

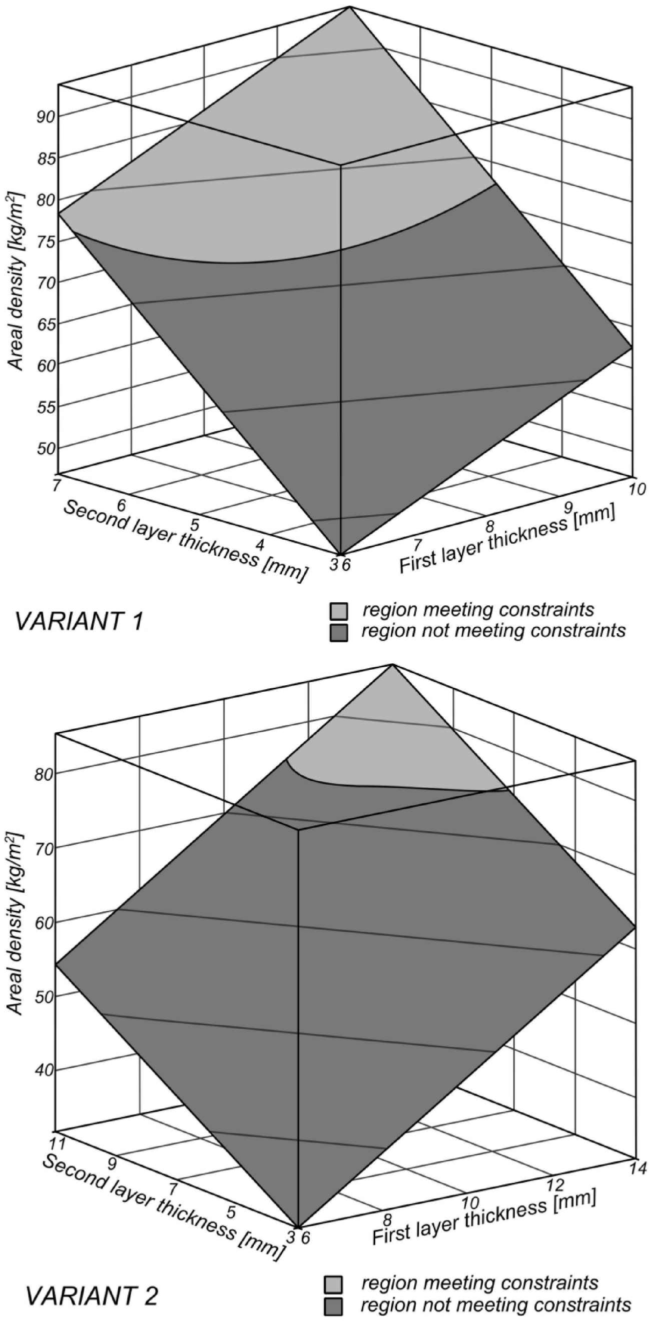

Fig. 5. Approximation of objective function

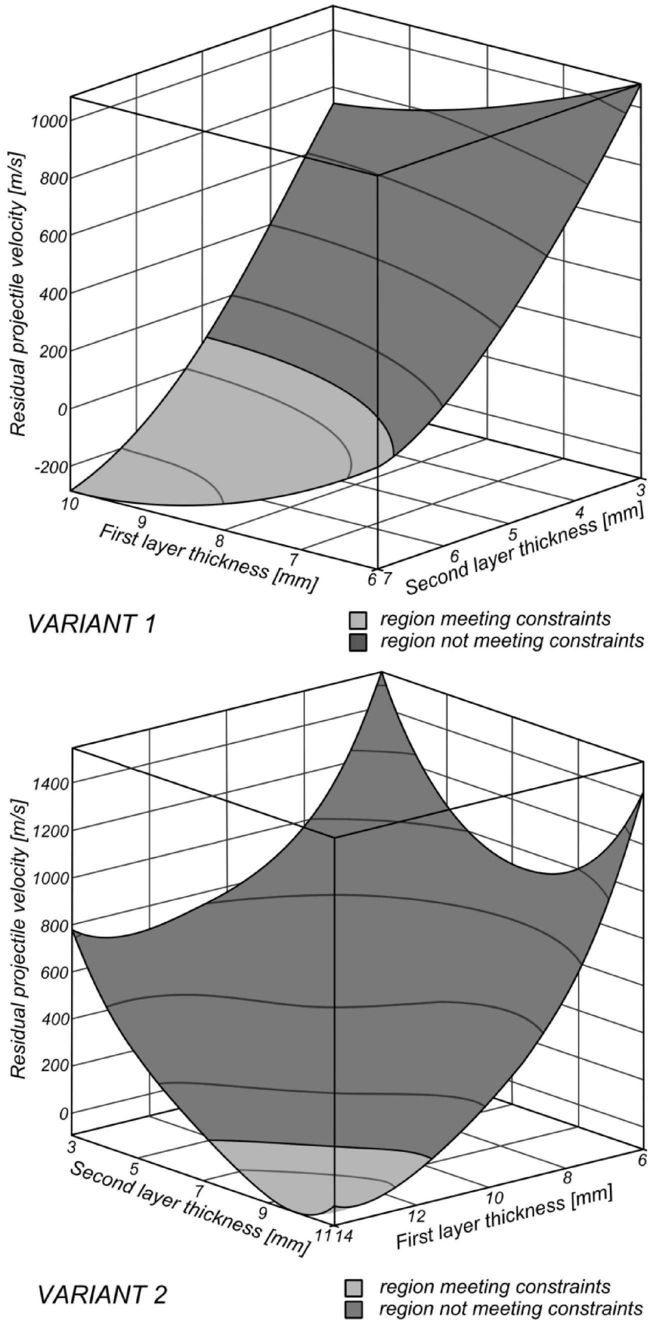

Fig. 6. Approximation of constraint function

Table 4
Results of two-layer armour optimization

	Variant	Optimal thickness [mm]		Residual projectile velocity [m/s]	Areal density [kg/m^2]
1	Al_2O_3 Armox 500T	Al_2O_3	7.35	5.64	71.07
		Armox 500T	5.42		
2	Al_2O_3 AA2024-T3	Al_2O_3	11.09	6.45	71.82
		AA2024-T3	10.20		

The layer thicknesses of the optimal panels for all cases and their corresponding values of both the objective and constraint function are listed in Table 4. The areal density of the armours considered as optimal for variants 1 and 2 are 71.07 and 71.82 kg/m^2, respectively. However, due to total thickness, a better solution is the armour in which the ceramic is supported by Armox 500T steel. Perforation of the variant recognized as optimal is shown in Fig. 7. Computed areal density is higher than the result obtained by Demir et al. [27], who investigated the ballistic protection of a panel consisting of alumina and 4340 steel against a 7.62×51 NATO AP projectile. Their studies reveal that even a panel with the areal density equal to 55 kg/m^2 is able to arrest the projectile. Shi and Grow [9] also determined that a two-component panel (Al_2O_3/AA6061) with the areal density of 53 kg/m^2 protects against a 7.62×51 mm NATO AP projectile. The reason of the difference is a low tensile strength of alumina used in the optimization process which is one of the most critical parameter deciding on ceramic effectiveness at the time of impact. Despite the reduced properties of alumina, the two-component panel still shows predominance in relation to the panel made entirely of Armox 500T steel, which, according to the experimental and numerical study of Kilic and Ekici [28], provides protection against a 7.62×54 B32 AP projectile with thickness and areal density greater than 13 mm and 100 kg/m^2, respectively.

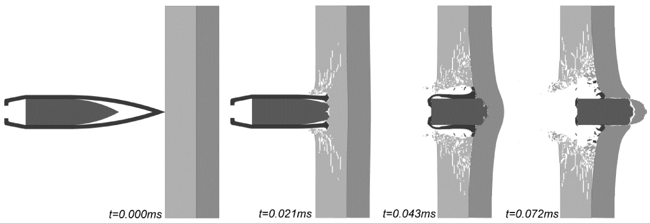

Fig. 7. Perforation of optimal panel

Validation. The optimization process was completed with validation of the obtained results. Al_2O_3-Armox 500T panel with the thickness of the alumina and steel layer equal to 7 and 6 mm was impacted by a 7.62x54 B32 AP projectile. A difference in layer thicknesses between the optimal and test variant resulted from a technological reason, however, an arrangement selected for validation contained within the set of feasible solutions defined by a constraint function and presents areal density comparable to the optimal solution, namely 74.33 kg/m^2. In accordance with the constraint function presented in Fig. 6, a projectile is arrested by a panel with selected parameters. In experimental test, no perforation was also observed, which proves that performed optimization was correct. Armour components before and after impact are depicted in Fig. 8. The ceramic layer was shattered during test. Therefore, it is not shown in Fig. 8 after projectile impact. A diameter of the real panel corresponded to a diameter of the numerical one. The measured velocity of the projectile was 834 m/s and it was close to the velocity in the numerical model.

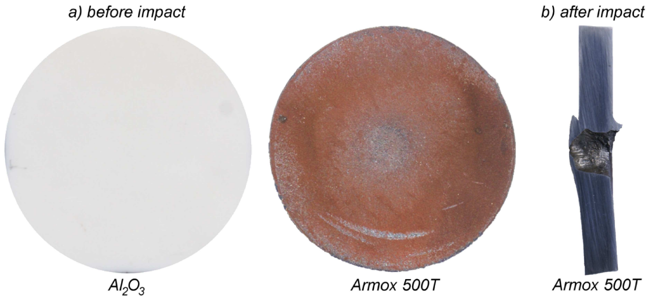

Fig. 8. Panel components before and after impact

4. Conclusions

The study resulted in the development of a panel optimization methodology, which allows the determination of the layer thicknesses of a panel with minimum areal density meeting the constraint in the form of the maximum velocity of the projectile after panel perforation. The conducted optimization process demonstrated that the areal density of a two-component panel is 71.07 and 71.82 kg/m^2 for Al_2O_3-Armox 500T and Al_2O_3-AA2024-T3, respectively. At the same time it was noted that tensile strength of ceramic is one of the key factors deciding on effectiveness of double-layer armour.

Acknowledgements. This work was supported by the National Centre for Research and Development, Poland [Grant No. O ROB 0001 03 001].

REFERENCES

[1] J. Lopez-Puente, A. Arias, R. Zaera, and C. Navarro, "The effect of thickness of the adhesive layer on the ballistic limit of ceramic/metal armours: an experimental and numerical study", *Int J. Impact Eng.* 32, 321–336 (2005).

[2] M.L. Wilkins, C.F. Cline, and C.A. Honodel, *Fourth Progress Report of Light Armour Program. Report UCRL 50694*, Lawrence Radiation Laboratory, Lawrance, 1969.

[3] R.M. Ogorkiewicz, "Development of lightweight armour system", *Proc. LASS* 1, CD-ROM (1995).

[4] P.J. Hazell, *Ceramic Armour: Design and Defeat Mechanisms*, Argos Press, Canberra, 2006.

[5] E. Lach and W.G. Pround, "Lightweight materials for passive light armour systems", *LWAG e- J.* 1, 1–14 (2006).

[6] A.L. Florence, *Interaction of Projectiles and Composite Armor. Part 2. Report No. AMMRC-CR-69-15*, Stanford Research Institute, Stanford, 1969.

[7] J.G. Hetherington, "Optimization of two-component composite armours", *Int. J. Impact Eng.* 12 (3), 409–414 (1992).

[8] B. Wang and G. Lu, "On the optimization of two-component plates against ballistic impact", *J. Mater. Proc. Technol.* 57, 141–145 (1996).

[9] J. Shi and D. Grow, "Effect of double constraints on the optimization of two-component armor systems", *Compos Struct* 79, 445–453 (2007).

[10] G. Ben-Dor, A. Dubinsky, and T. Elperin, "Improved Florence model and optimization of two-component armor against single impact or two impacts", *Compos Struct* 88, 158–165 (2009).

[11] A.A. Growenwold and J.A. Snyman, "Global optimization using dynamic search trajectories", *J. Global Optim.* 24, 51–60 (2002).

[12] N. Stander, W. Roux, T. Goel, T. Eggleston, and K. Craig, *LS-OPT User's Manual. A Design Optimization and Probabilistic Analysis Tool for the Engineering Analyst*, Livermore Software Technology Corporation, Livermore, 2010.
[13] M. Luzar, Ł. Sobolewski, W. Miczulski, and J. Korbicz, "Prediction of corrections for the Polish time scale UTC (PL) using artificial neural networks", *Bull. Pol. Ac.: Tech.* 61 (3), 589–594 (2013).
[14] C.T. Kowalski and M. Kamiński, "Rotor fault detector of the converted-fed induction motor based on RBF neural network", *Bull. Pol. Ac.: Tech.* 62 (1), 69–76 (2014).
[15] H.E. Romeijn and R.L. Smith, "Simulated annealing and adaptive search in global optimization", *Probab. Eng. Inf. Sci.* 8, 571–590 (1994).
[16] J.A. Snyman, "The LFOPC leap-frog algorithm for constrained optimization", *Comput. Math. Appl.* 40, 1085–1096 (2000).
[17] W. Moćko and Z.L. Kowalewski, "Perforation test as an accuracy evaluation tool for a constitutive model of austenitic steel", *Arch Metall. Mater.* 58 (4), 1105–1110 (2013).
[18] M. Jutras, "Improvement of the characterization method of the Johnson-Cook model", *Master Thesis*, Laval University, Laval, 2008.
[19] M. Nilsson, *Constitutive Model for ARMOX 500T and ARMOX 600T at Low and Medium Strain Rates. Technical Report FOI-R-1068-SE*, Swedish Defence Research Agency, Stockholm, 2003.
[20] W.J. Kury, D. Breithaupt, and M.C. Tarver, "Detonation waves in trinitrotoluene", *Shock Waves* 9, 227–237 (1999).
[21] B. Adams, "Simulation of ballistic impacts on armored civil vehicles", *Master Thesis*, Eindhoven University of Technology, Eindhoven, 2003.
[22] V. Panov, "Modelling of behaviour of metals at high strain rates", *PhD Thesis*, Cranfield University, Cranfield, 2006.
[23] T. Wierzbicki, Y. Bao, Y.W. Lee, and Y. Bai, "Calibration and evaluation of seven fracture models", *Int. J. Mech. Sci.* 47, 719–743 (2005).
[24] D.S. Cronin, K. Bui, C. Kaufmann, G. McIntosh, and T. Berstad, "Implementation and validation of the Johnson-Holmquist ceramic material model in LS-Dyna", *Proc. 4th Eur. LS-DYNA Users Conf.* 1, 47–60 (2003).
[25] T. Li, F. Grignon, D.J. Benson, K.S. Vecchio, E.A. Olevsky, F. Jiang, A. Rohatgi, R.B. Schwarz, and M.A. Meyers, "Modeling the elastic properties and damage evolution in Ti-Al_3Ti metal-intermetallic laminate (MIL) composites", *Mater. Sci. Eng.* A 374, 10–26 (2004).
[26] A. Tasdemirci and I.W. Hall, "Numerical and experimental studies of damage generation in multi-layer composite materials at high strain rates", *Int. J. Impact Eng.* 34, 189–204 (2007).
[27] T. Demir, M. Ubeyli, R.O. Yildirim, and M.S. Karakas, "Investigation of the ballistic performance of alumina/4340 steel laminated composite armor against 7.62 armor piercing projectiles", *Proc. 17th Int. Metallurgical & Materials Conf.* 1, 1–7 (2008).
[28] N. Kiliç and B. Ekici, "Ballistic resistance of high hardness armor steels against 7.62 mm armor piercing ammunition", *Mater Design* 44, 35–48 (2013).